J. Fluid Mech. (2024), *vol*. 988, A51, doi:10.1017/jfm.2024.450

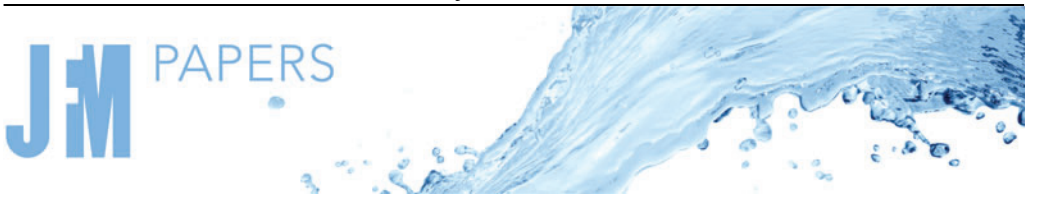

Spreading of a viscoelastic drop on a solid substrate

Peyman Rostami[1],†, Mathis Fricke[2], Simon Schubotz[1,3], Himanshu Patel[1], Reza Azizmalayeri[1] and Günter K. Auernhammer[1],†

[1]Leibniz-Institut für Polymerforschung Dresden e.V. Hohe Straße 6, 01069 Dresden, Germany

[2]Department of Mathematics, TU Darmstadt, Schlossgartenstraße 7, 64289 Darmstadt, Germany

[3]TU Dresden, Dresden 01062, Germany

(Received 31 August 2023; revised 19 April 2024; accepted 28 April 2024)

We study the spreading of Newtonian viscous (aqueous glycerin solution) and viscoelastic (aqueous polymer solution) drops on solid substrates with different wettabilities. For drops of the same zero-shear viscosity, we find in the early stages of spreading that viscoelastic drops (i) spread faster and (ii) their contact radius shows a different power law vs time than Newtonian drops. We argue that the effect of viscoelasticity is only observable for experimental time scales of the order of or larger than the internal relaxation time of the viscoelastic polymer solution. We attribute this behaviour to the shear thinning of the viscoelastic polymer solution. When approaching the contact line, the shear rate increases and the steady-state viscosity of the viscoelastic drop is lower than that of the Newtonian drop. We support our experimental findings with a simple (first-order) perturbation model that qualitatively agrees with our findings.

Key words: drops, wetting and wicking, viscoelasticity

1. Introduction

For at least the last two centuries, the interaction of droplets with surfaces has been studied quantitatively. By way of a retrospective, outstanding work was done by Young for static wetting (Young 1805) and Worthington for drop impact (Worthington Arthur & Reynolds 1883) and drop spreading over different surfaces (Hardy 1919; Shuttleworth & Bailey 1948; Fox & Zisman 1950). Drop spreading and its dynamics play an essential role in many industrial applications, from printing to coating (Sankaran & Rothstein 2012; Hoath 2016; Glasser *et al.* 2019). The spreading of Newtonian drops has been the subject of extensive research over the last two decades (de Gennes 1985; Biance, Clanet & Quéré 2004; Bird,

† Email addresses for correspondence: rostami@ipfdd.de, auernhammer@ipfdd.de

Mandre & Stone 2008; Bonn *et al.* 2009; Muralidhar *et al.* 2011; Snoeijer & Andreotti 2013). For low-viscosity drops, the key finding is that the spreading dynamics consists of two regimes; an inertial and a viscous dominated regime (Biance *et al.* 2004).

The boundary condition has an important influence on the calculation of the flow field close to the contact line and thus on the viscous dissipation. By assuming a no-slip condition, the contact line motion is solved by Moffatt (1964). The assumption of the no-slip condition leads to a logarithmic divergence of the viscous stress due to the hydrodynamic singularity at the moving contact line (Huh & Scriven 1971; Huh & Mason 1977; Tanner 1979; Fricke, Köhne & Bothe 2019; Fricke & Bothe 2020). Various solutions have been proposed to this problem in molecular-scale (Blake & Haynes 1969; Cherry & Holmes 1969; Ruckenstein & Dunn 1977), hydrodynamic models by Cox (1986), Voinov (1976) and Shikhmurzaev (1997, 2020) and by including evaporation and condensation (Wayner 1994; Shanahan 2001; Rednikov & Colinet 2012). For the fast processes, the dynamics can be modelled by a hydrodynamic model with a slip length that generates a lower cutoff length below which the liquid and solid velocities are allowed to differ in the vicinity of the contact line and/or the substrate.

Consider a drop of initial radius R (when hanging at the needle), volume V, density ρ, viscosity η and surface tension σ which gently touches a solid substrate; it starts spreading with velocity of u. In the early stage of spreading, inertia is assumed to be dominant (Biance *et al.* 2004). By writing a force balance between inertial $(\mathrm{d}/\mathrm{d}t)((\rho V)u)$ and capillary forces $\sim \sigma r$, one can derive the spreading rate, (1.1), where the radius of the wetted on the substrate area is r

$$\left(\frac{r}{R}\right)^2 = t\sqrt{\frac{\sigma R^3}{\rho}}. \tag{1.1}$$

In a second regime, the viscous dissipation near the contact line is the rate-limiting process when the drop shape is close to a spherical cap. For the viscous dominated regime (Tanner regime) of drop spreading, the Cox–Voinov relation for the dynamic contact angle in the case of perfect wetting is $\theta^3 \sim \eta(u/\sigma)$, and the conservation of volume, $r^3\theta \sim V$, results in the spreading dynamics being in the viscous regime. This relation is known as Tanner's law (Tanner 1979)

$$r \sim R\left(\frac{\sigma t}{\eta R}\right)^{1/10}. \tag{1.2}$$

In general, drop spreading often follows a power law $r \sim t^{\alpha}$ with spreading exponent α that depends on various parameters. It should be noted that the Cox–Voinov relation was originally developed for a final contact angle $\theta = 0$, but was later shown to be valid for higher contact angles of up to 100° (Fermigier & Jenffer 1991; Petrov *et al.* 2003). By equating the radius from the inertial and viscous regimes, the transition between these two regimes can be calculated: $\tau_{iv} \sim (\rho\sigma R/\eta^2)^{1/8}\sqrt{\rho R^3/\sigma}$ (Biance *et al.* 2004). The above models work reasonably well for low-viscosity drops (e.g. water). For the early stages of high-viscosity drop spreading, there are several conflicting results (Carlson, Bellani & Amberg 2011, 2012; Eddi, Winkels & Snoeijer 2013). Carlson *et al.* (2012) stated that the drop-spreading dynamics still follows the power-law type of spreading with the same exponent but with a friction factor (μ_f) as a correction factor for the prefactor of the power law, $r/R \sim (\sigma t/R\mu_f)^{1/2}$. Eddi *et al.* (2013) argue that, for highly viscous liquids, the inviscid solution is not valid anymore, so they solve for Stokes flow in this case. An important approach is to use the assumed analogy between the merging of identical drops

(Eggers, Lister & Stone 1999) and the spreading of drops on a substrate. Eddi *et al.* (2013) used a logarithmic model to scale their experimental data $r \simeq -(1/4\pi)(\sigma/\eta)t\ln(r/R)$.

Viscoelastic materials combine an elastic component and a viscous component in their properties. When a polymer solution is sheared, at very short times only the elastic part contributes to the dynamics and after a characteristic time the viscous part becomes relevant (Costanzo *et al.* 2016). To observe the effect of viscoelasticity, the experimental time scale should be of the order of the viscoelastic time scale, i.e. polymer relaxation time. In a simple approach, the viscosity of polymer solutions can be described by the Cross model (Cross 1965; Subbaraman, Mashelkar & Ulbrecht 1971; Gastone, Tosco & Sethi 2014). When shear is applied to a viscoelastic material, it takes several times the relaxation time of the sub-chain to reach a steady state. The relaxation time depends on the polymer concentration or/and molar mass (number of entanglements) (Costanzo *et al.* 2016; Vereroudakis *et al.* 2023)

$$\eta = \frac{\eta_0 - \eta_\infty}{1 + (\tau_{ve}\dot{\gamma})^m} + \eta_\infty. \tag{1.3}$$

Here, $\dot{\gamma}$ is the shear rate, τ_{ve} and m are fluid parameters (polymer relaxation time and rheological exponent) and η_0 and η_∞ are the zero and infinite shear rate viscosities, respectively. By increasing the polymer concentration and/or polymer molar mass, the polymer relaxation time τ_{ve} increases and the rheological exponent m decreases (see supplementary material available at https://doi.org/10.1017/jfm.2024.450).

Despite many industrial applications (e.g. printing), the early drop spreading of viscoelastic fluids has not been extensively studied. Some studies focus on the impact of viscoelasticity of the soft substrates underneath spreading macroscopic (Chen, Auernhammer & Bonaccurso 2011; Chen, Bonaccurso & Shanahan 2013*a*) and static nanoscopic drops (Zhao *et al.* 2021). In the case of wetting and dewetting on a viscoelastic substrate, it is shown that the wetting and dewetting dynamics depends directly on the mechanical properties of the substrate (Carré, Gastel & Shanahan 1996; Carré & Shanahan 2001). In most of the studies regarding viscoelastic drop spreading, the viscous dominated regime (late stage of drop spreading) is studied experimentally, theoretically and numerically (Carré & Eustache 2000; Betelu & Fontelos 2003; Liang *et al.* 2009; Iwamatsu 2017; Jalaal, Stoeber & Balmforth 2021). The viscous spreading exponent (α) is correlated with the rheological exponent n in these models. Only very recently has the early stage of drop spreading of shear thinning fluids been studied by two groups (Bouillant *et al.* 2022; Yada *et al.* 2023). Both groups reported that the early stage of drop spreading (regardless of polymer concentration and molar mass) shows the same spreading exponent as low-viscosity drop spreading (e.g. water drops). The considered time scales of experiments in both cases are below the inertia–capillary time ($\tau_{ic} = \sqrt{\rho R^3/\sigma}$), which is of the order of a few milliseconds for millimetric drops.

In this contribution, we follow the hypothesis that three time scales should be considered; the inertia–viscous (τ_{iv}) cross-over time, the inertia–capillary cross-over time (τ_{ic}) and the polymer relaxation time (τ_{ve}). To illustrate these time scales, we calculate them for water and an aqueous polyethylene oxide (PEO) solution (4 %(w/w)) with a molar mass of $(6 \times 10^5 (\mathrm{g\,mol^{-1}}))$. For a millimetric water drop we get $\tau_{iv} \sim 15$ ms, $\tau_{ic} \sim 3.7$ ms and $\tau_{ve} \sim 0$, and for the polymer solution $\tau_{iv} \sim 2.8$ ms, $\tau_{ic} \sim 4$ ms and $\tau_{ve} \sim 22$ ms. The polymer relaxation time can be larger or smaller than the time scales of drop spreading. In this contribution, we study some effects of changes of the order of these time scales and provide a simple model to rationalize our findings.

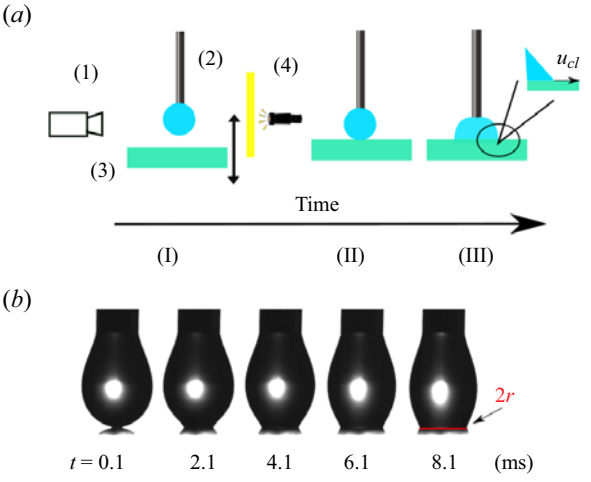

Figure 1. (*a*) Sketch of the drop-spreading set-up, with a high-speed camera (1), cold light source and diffuser sheet (4), drop and needle (2) and the adjustable solid substrate (3). Different stages of spreading are illustrated over time, (I) before contact between substrate and the drop (II) the substrate is gently coming up and the drop touches the substrate (the initial point of contact). (III) After contact and spreading of the drop on the substrate with contact line velocity of u_{cl}. (*b*) The spreading dynamics of a millimetric drop over a hydrophilic substrate for different times; the spreading radius r is shown.

2. Experimental method

The droplet dispenser is set up so that the drop hangs from a dull needle (outer diameter 2.1 mm) and the substrate is lifted up gently until it touches the drop. After contact, the drop spreads immediately. The drop spreading is recorded in side view by a high-speed camera (FASTCAM Mini AX 200, Photron) equipped with a Navitar objective (12X). The test section is illuminated by an LED cold light source (SCHOTT KL 2500) through a diffuser sheet, giving a homogeneous back illumination (figure 1). All drop-spreading experiments were performed in a laboratory with controlled environmental conditions (temperature 23 °C, relative humidity 48 %).

Water (MicroPure UV/UF, Thermo Scientific Co.), glycerin (Sigma Aldrich co. 99 %) and mixtures thereof as well as water–PEO (Sigma Aldrich co.) solutions of various molar masses and concentrations are used as Newtonian and viscoelastic operating fluids, respectively. For the aqueous PEO solutions, from now on, the weight concentrations are shown as per cent (%) and the molar masses of polymers are mentioned as k, which is 10^3 g mol^{-1} . The sample names and viscosities at zero shear rate (zero shear viscosity) for each liquid are given in table 1. The surface tension σ of all samples is in the range of $63 \leq \sigma \leq 72$ mN m^{-1}. To measure the flow curves, a commercial rheometer (MCR 502, Anton-Paar GmbH) is used. For all measurements a cone–plate geometry is used with a diameter of 50 (mm) and cone angle of 1° and the gap of 100 µm (CP50-1). In the rheological experiments the temperature of the sample was kept constant at 23 °C. The rheological properties of each sample are given in the supplementary material (figure S2). As substrates we used glass substrates, with two different types of surface preparations. Cleaned glass substrates as hydrophilic substrates (contact angle of water drop around 15°) and silanized glass substrates as hydrophobic substrates (contact angle of water drop around 90°) are used. Details of substrate preparation are given in the supplementary material and previous work (Rostami *et al.* 2023). When preparing polymer solutions, it is crucial to wait long enough for the polymer to dissolve homogeneously in the

Sample	Molar mass (10^3 g mol^{-1})	η_0 (mPa s)	Sample	η_0 (mPa s)
Water + PEO (2 %, 300*k*)	300	35 ± 0.5	Water + Glycerin (0 %)	0.93 ± 0.01
Water + PEO (3 %, 300*k*)	300	101 ± 0.5	Water + Glycerin (72 %)	35 ± 0.5
Water + PEO (4 %, 300*k*)	300	254 ± 0.5	Water + Glycerin (85 %)	98 ± 0.5
Water + PEO (2 %, 600*k*)	600	103 ± 0.5	Water + Glycerin (91.5 %)	293 ± 0.5
Water + PEO (3 %, 600*k*)	600	537 ± 0.5	Water + Glycerin (93.5 %)	389 ± 0.5
Water + PEO (4 %, 600*k*)	600	1324 ± 0.5	Water + Glycerin (100 %)	1078 ± 0.5

Table 1. Composition of operating fluids and the zero-shear viscosity η_0 (at 23 °C). The rheological properties of each sample are given in the supplementary material.

solution. This is illustrated by our rheology experiments. For high molar masses, we measured changes in the flow curves within the first month after preparing the sample (see supplementary material).

3. Spreading of viscoelastic and viscous Newtonian drops

3.1. *Hydrophilic substrates*

In figure 2(*a*), we plot the time dependence of the radius of the wetted area (r) normalized to the initial drop radius (R) for viscous Newtonian (water–glycerol mixture) and viscoelastic drops on a hydrophilic substrate. One of the challenges of plotting the spreading radius over time is to determine the time of the first contact. Three options have been suggested to overcome this problem. The simplest solution to add a bottom view camera and capture the contact areas from the bottom (Eddi *et al.* 2013) and to record at very high frame rates. Plotting the contact line velocity against the dimensionless spreading radius (r/R) is another possible approach (Hartmann *et al.* 2021). The advantage of the latter method is that it does not need a definition of zero time (see supplementary material). The third option is to define a fitting parameter as t_0; this parameter can pop up in the fitting function $r = B(t - t_0)^{\alpha}$. In all our experiments, this parameter is of the order of a few frames $t_0 \sim 0.0001$ s. In all plots data points for times below $t \approx 0.5$ ms are omitted to be sure that the definition of the first contact time has no influence on the fit. Consequently, we fitted the drop-spreading results from the fifth data point to $t = 20$ ms; this time range in our study is defined as the 'early stage' of drop spreading. This time scale is of the order of the cross-over time scale (from the inertial regime to the viscous regime) defined by Biance *et al.* (2004) and 7 times higher than the characteristic time scale defined by Bouillant *et al.* (2022) ($t = 3$ ms).

As expected from (1.1), a viscous Newtonian drop spreads in a manner proportional to square root of time, $r \sim \sqrt{t}$. However, viscoelastic drops (aqueous PEO solutions) spread with different spreading exponents ($r = Bt^{\alpha}$ with $\alpha < 0.5$). To illustrate this difference, two samples, here 'Water + PEO(3 %, 300*k*)' *and* 'Water + Glycerin (85 %)' ($\eta_0 \approx$ 100 mPa s), with the same zero-shear viscosity and the same initial drop size (defined by the image processing method and double checked with the drop volume, $D \approx 4$ mm), density and surface tension ($\sigma \approx 65$ mN m^{-1}) have clearly different spreading exponents α (figure 2*a*). This does not match the existing models if we assume that the viscosity of the viscoelastic liquid is equal to its zero-shear viscosity at all times. Under this assumption, the Newtonian and viscoelastic liquids should spread with an identical dynamics. For the same prefactor in the power law, see figure 2(*d*), a smaller spreading exponent (α) (for $t \leq 0.02$ s) results in higher spreading rates.

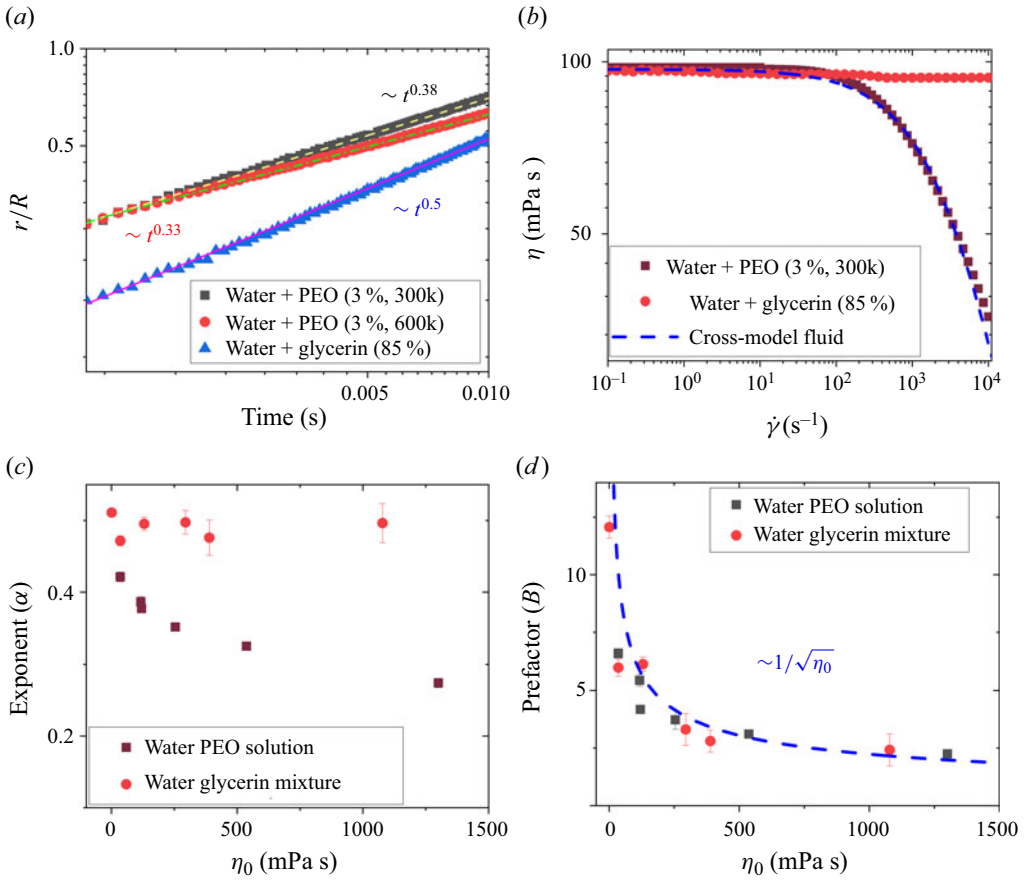

Figure 2. (*a*) Radius of the wetted area (r) normalized by the initial radius of the drop (R) as a function of time, for water and PEO (3 %, 300k and 3 %, 600k) and water and glycerin (85 %) on hydrophilic substrates. (*b*) Flow curve of an aqueous PEO (3 %, 300k) solution and a water–glycerin mixture (85 %). (*c*,*d*) Spreading exponent (α) and spreading prefactor as a function of the zero-shear viscosity η_0 for all viscous Newtonian and viscoelastic liquids mentioned in table 1.

To illustrate the effect of viscoelasticity, we use a typical flow curve of PEO solutions. The viscosity at low shear rates remains constant. Above a certain critical shear rate, the viscosity decays with increasing shear rate. Such a behaviour can be described by the Cross-fluid model (1.3). In contrast, water–glycerin mixtures show no evidence of shear thinning in our data; see figure 2(*b*). However, this may occur at even higher shear rates (Dontula, Macosko & Scriven 1999). The shear rate at which the viscosity differs from its zero shear value defines an internal relaxation time of the polymer solution, τ_{ve} in (1.3).

Our hypothesis is that the spreading dynamics depends on the rheological properties of the operating fluid. The velocity of the contact line in this early regime of drop spreading is of the order of $u_{cl} \sim 1$ m s^{-1}. In the case of a no-slip boundary condition the stress and viscous dissipation at the three phase contact point diverges (this is known as the 'Huh–Scriven paradox' Huh & Scriven 1971). Although the viscous dissipation is expected to be effective up to the capillary length (Snoeijer *et al.* 2005; Pelosse, Guazzelli & Roché 2023), it is shown that the density of viscous dissipation is much higher in the vicinity of the three phase contact point than the rest of the drop (Bodziony, Wörner & Marschall

2023; Li *et al.* 2023). If we consider a distance d in the range of 1 μm to 1 mm from the contact line, the shear rate $\dot{\gamma} = u_{cl}/d$ can be estimated to be of the order of 10^3–10^6 s^{-1}.

Thus, for the early stage of drop spreading, two effects have to be taken into account: the shear-rate dependence of the steady-state viscosity and the time dependence of the viscosity (Costanzo *et al.* 2016; Vereroudakis *et al.* 2023). In the supporting information, figure S5, we show the cross-over between a phase in which viscoelasticity is not yet contributing to drop spreading and a phase in which viscoelasticity contributes to the spreading dynamics. For the moment, we focus on the phase in which viscoelasticity contributes to drop spreading. For a more detailed discussion of this cross-over see § 4. At the high shear rates in the vicinity of the moving contact line, the viscosity of the polymer solutions decreases significantly, figure 2 and S2. However, the viscosity of a Newtonian liquid remains more or less constant. This implies that, in the Newtonian case, the effective viscosity near the contact line is higher. Following earlier works that see an influence of viscosity on the early stage of drop spreading (Carlson *et al.* 2011, 2012; Eddi *et al.* 2013), we come to the following qualitative picture: the dissipation close to the contact line is higher in the Newtonian case than the viscoelastic case, leading to a lower contact line velocity, which is in good agreement with our experimental results.

To test our hypothesis, we measure the spreading exponent and the spreading prefactor over a wide range of zero-shear viscosities and rheological properties for viscous Newtonian and viscoelastic drops spreading on hydrophilic substrates, (figures 2*c* and 2*d*). The initial observations are verified by this systematic variation of the material parameters. For viscous Newtonian fluids, the spreading exponent is slightly decreasing with increasing zero-shear viscosity, $\alpha \approx 0.5$ on the hydrophilic substrates. In contrast, for viscoelastic fluids, the spreading exponent is a strongly decreasing function of the zero-shear viscosity, (figure 2*c*). This difference is an indication of the dependence of the spreading exponent (α) on the rheological properties. The trend of the spreading prefactor seems to depend only on the zero-shear viscosity but not on the rheological exponent (figure 2*d*). The spreading prefactor (for Newtonian and viscoelastic cases) roughly follows $B \sim {\eta_0}^{-0.5}$, figure 2(*d*), which was also observed previously (Carlson *et al.* 2011; Eddi *et al.* 2013).

3.2. *Effect of substrate's wettability*

Repeating the spreading experiments for Newtonian and viscoelastic liquids on hydrophobic substrates (i.e. $\theta_0 \simeq 90°$) reveals a number of important observations; see figure 3. (i) On average, the spreading exponent (α) decreases as the contact angle increases. (ii) The spreading exponent remains almost independent of the zero-shear viscosity for Newtonian drops. (iii) Increasing the zero-shear viscosity of viscoelastic liquids (i.e. increasing the concentration and/or molar mass of the polymer) reduces the exponent. The difference between the spreading of Newtonian and viscoelastic drops shows the same trend regardless of the hydrophobicity of the substrate. To summarize our experimental results, the spreading exponent is dependent on the viscoelasticity of the drop and the prefactor is a function of viscosity. All of the developed models up to now cannot predict the effect of viscoelasticity. In the next sections we first discuss this in more detail and then present a simplistic model to predict this behaviour.

4. Transition from the viscoelastic to the elastic case

The results presented so far show a clear dependency of drop spreading on the viscoelasticity of the drop liquid. An important point here is the apparent contradiction

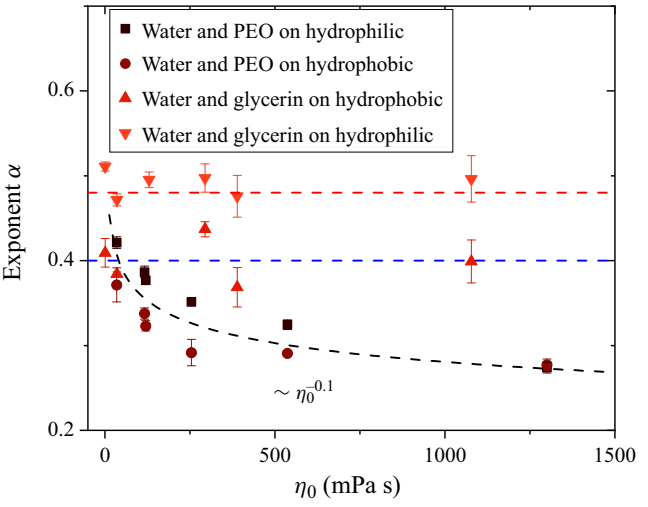

Figure 3. Experimental spreading exponent (α) as a function of the zero-shear viscosity η_0 for viscous Newtonian ('Water and glycerin') and viscoelastic liquids ('Water and PEO') on hydrophobic and hydrophilic substrates.

between our results and previous published works by two other groups (Bouillant *et al.* 2022; Yada *et al.* 2023). These groups stated that the concentration of polymer solutions does not change the dynamic of the drop spreading compared with water as the drop liquid and the exponent remains constant at $\alpha = 0.5$. Both groups used PEO (4×10^6 g mol^{-1}) up to 2 % in weight concentration. So far we have considered intermediate polymer molar masses (300×10^3 g mol^{-1} and 600×10^3 g mol^{-1}) and concentrations. In the following part of this section we discuss the differences between the present work and the works by Bouillant *et al.* (2022) and Yada *et al.* (2023) in detail.

In the early stage of the viscoelastic drop spreading, capillary and inertia forces are very similar for all used liquid (Newtonian and non-Newtonian). However, as a function of time (or alternatively frequency), there is an interplay between the viscous and elastic contributions in the non-Newtonian polymer solutions. Especially for short times ($t \ll \tau_{ve}$), the elastic contributions dominate and only for long enough times ($t \gg \tau_{ve}$) do the viscous contributions take over. The characteristic time of this cross-over is influenced by the polymer molar mass and concentration. The non-dimensional number which takes into account this interplay in our wetting situation is the elastocapillary number (Ec). Previously, Ec was used for the liquid breakup of polymer solutions (Anna & McKinley 2001). The elastocapillary number Ec is the ratio of the polymer relaxation time (τ_{ve}) to the viscous–capillary time scale $t_{vc} = \eta d/\sigma$ (McKinley 2005), where d is the characteristic length. If we consider the characteristic length as the initial drop radius (R_0) and the viscosity as the zero-shear-rate viscosity (η_0), we can rewrite the elastocapillary number as (4.1)

$$Ec = \frac{\sigma \tau_{ve}}{\eta_0 R_0}. \tag{4.1}$$

The critical value for this number is unity ($Ec = 1$). For very small $Ec \ll 1$, the liquid is purely viscous. By increasing Ec, the elasticity is increasingly important. In the limit $Ec \gg 1$, the flow is elastically dominated (McKinley 2005). For the intermediate polymer masses we have used so far, the elastocapillary number ranges between $Ec = 0.05$ and $Ec = 0.5$ (table 2). An effective way to increase Ec is to increase the molar masses of polymer.

Sample	Molar mass (10^3 g mol^{-1})	η_0 (mPa s)	τ_{ve} (s)	Ec
Water + PEO (3 %, 300k)	300	101 ± 0.5	0.0002186	0.07
Water + PEO (3 %, 600k)	600	537 ± 0.5	0.004355	0.26
Water + PEO (4 %, 600k)	600	1324 ± 0.5	0.02218	0.54
Water + PEO (1 %, 1000k)	1000	54 ± 0.5	0.002646	1.59
Water + PEO (2 %, 1000k)	1000	495 ± 0.5	0.0162	1.06
Water + PEO (3 %, 1000k)	1000	3340 ± 0.5	0.0942	0.92
Water + PEO (0.25 %, 8000k)	8000	210 ± 0.5	0.288	44.5
Water + PEO (0.5 %, 8000k)	8000	2450 ± 0.5	2.31	30.5

Table 2. Composition of operating fluids, the zero-shear viscosity η_0 (at 23 °C), the polymer relaxation time τ_{ve} (s) based on a fit to the Cross model (1.3) and the respective elastocapillary number Ec (4.1).

We prepared two other set of liquids with higher molar masses of (1×10^6 g mol^{-1} and 8×10^6 g mol^{-1}), the zero-shear-rate viscosities (η_0), polymer relaxation time (τ_{ve}) and respective elastocapillary numbers (Ec) are listed in the table 2.

For the high molar masses, the drop spreading consists of two regimes. At short times ($t < 2$ ms) the drop spreads with an exponent close to 0.5. Later, at longer times, the exponent decreases (see supplementary material figure S5). All data shown so for the lower molar masses were in this second regime.

Plotting the spreading exponent as a function of elastocapillary number Ec reveals that, for $Ec < 1$, the exponent decreases with increasing Ec (increasing the elasticity of liquid). By increasing the elastocapillary number, $Ec > 1$, the exponent increases with increasing Ec and reaches a plateau region for $Ec \gtrapprox 2$. Since the elastocapillary number is the ratio of the polymer relaxation time to the wetting time scale (the viscous capillary time scale), the higher value of the elastocapillary number implies that the relaxation time scale of the polymer is longer than the wetting time scale. In other words: to observe the effects of the viscosity of the polymer solution, the experimental time scale must be of the order of the polymer relaxation time. So for high values of the elastocapillary number, $Ec \gtrapprox 2$, the elasticity dominates. It can be anticipated that this regime behaves close to the inviscid case. The dependency on Ec is the same for hydrophilic and hydrophobic substrates (figure 4).

In the previous studies (Bouillant *et al.* 2022; Yada *et al.* 2023), the elastocapillary numbers were not reported. However, based on their measurements for low concentration ($c = 0.1wt\%$), Ec is probably very low ($Ec \ll 1$). In contrast, for higher concentrations, the Ec was probably above the threshold ($Ec \gtrapprox 2$). In both extremes, Bouillant *et al.* (2022) and Yada *et al.* (2023) could hardly observe the effect of viscoelasticity.

5. A first-order model

5.1. *Inviscid case*

For low-viscosity drops, increasing the hydrophobicity of the substrate (by suitable surface modification of the substrate) results in a decreasing spreading rate and exponent (Bird *et al.* 2008; Chen *et al.* 2013*b*; Du *et al.* 2021). This was explained in terms of a simple energy balance. This balance assumes that no energy is dissipated ($\mathrm{d}e/\mathrm{d}t = 0$). In this approximation, the kinetic energy (left-hand side of (5.1)) is balanced by a combination of free surface energy and wetting energy (right-hand side of (5.1), Bird *et al.* 2008).

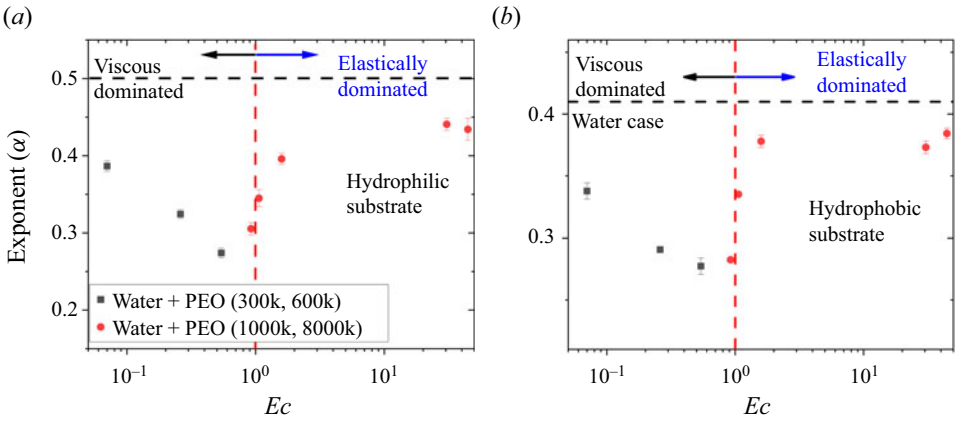

Figure 4. (*a*) The early stage of drop spreading exponent (α) as a function of elastocapillary number (Ec) for intermediate molar masses (300×10^3 and 600×10^3 (g mol^{-1}), black squares) and high molar masses (1000×10^3 and 8000×10^3 (g mol^{-1}), red circles) on a hydrophilic substrate and (*b*) on a hydrophobic substrate. The black dashed lines show the exponent for water on the substrate and red dash lines illustrate the elastocapillary number $Ec = 1$.

This model makes a couple of assumptions that allow us to adapt it for our first-order approach

(i) The change in surface area of the drop scales with $r(t)^2$: $A(0) - A(t) \approx \pi F(\theta_0) r(t)^2$.
(ii) The flow field is assumed to be self-similar with a characteristic length scale that scales as $l_{(ci)} \sim (\gamma t^2/\rho)^{(1/3)}$.

$$\int_V \frac{1}{2}\rho u^2 \, \mathrm{d}V = \sigma[A(0) - A(t) + \pi r(t)^2 \cos(\theta_0)]. \tag{5.1}$$

Here, u is the velocity field inside the drop, ρ is the liquid density, $A(t)$ and $A(0)$ are the surface area of the liquid–vapour interface during the spreading and at the time zero and θ_0 is the contact angle at which the drop spreading would stop, i.e. the static advancing contact angle. Bird *et al.* (2008) solved the balance equation (by modelling the kinetic energy integral) and showed that the spreading is a function of the substrate's wettability (5.2)

$$r(t) = c_1 t^{\alpha}. \tag{5.2}$$

In this solution, the spreading exponent is $\alpha = c_2\sqrt{F(\theta_0) + \cos(\theta_0)}$, where the unknown function F depends weakly on θ_0 (see Bird *et al.* 2008). As the contact angle increases, the spreading exponent decreases. Our experiments show the same behaviour (figure 3).

5.2. *Including viscous dissipation*

Above a certain viscosity of the drops, viscous dissipation cannot be neglected. Hydrodynamic models like the Moffatt (1964) solution suggest that the viscous dissipation is of the order of $\sim 2\pi\eta r u^2$. The dissipation rate (j_e^D) is balanced by the rate of change of the total energy ($\mathrm{d}e/\mathrm{d}t = j_e^D$). We add the dissipation term to the left-hand side of the time derivative of (5.1). In doing so, we keep the assumptions (i) and (ii) as mentioned in the previous section. Additionally, we assume that (iii) the scaling of the characteristic length scale does not change due to viscous effects.

Approximation (iii) actually is a consequence of the first-order character of our model and will limit our model to not too high viscosities. To solve the resulting equation (5.3), we assume the viscous term to be small ($\eta \to \epsilon\eta^*$) and to act as a perturbation term (the first-order perturbation model). From now on we drop all explicit mention of time as an argument

$$2\pi\sigma\{\tfrac{1}{2}t\dot{r}^2 + \tfrac{1}{2}t^2\ddot{r} - r\dot{r}[F(\theta_0) + \cos(\theta_0)]\} = -2\pi\epsilon\eta^* r\dot{r}^2. \tag{5.3}$$

We rewrite equation (5.3) in dimensionless units ($t = \tau_{ve}\hat{t}$, $r = r^*\hat{r}$). After simplification (5.3) can be rewritten as (5.4). Here, the elastocapillary number pops up again, which confirms that this non-dimensional number is relevant, $Ec = \sigma\tau_{ve}/\eta r$. In our perturbation approach, it is convenient to have Ec on the right side. We actually use the inverse of Ec, as $Ec^* = \eta^* r^*/\sigma\tau_{ve} = 1/Ec$. Taking typical values for the viscosity of the liquids ($\eta^* \sim 100$ mPa s), the length scale as the initial drop radius ($r^* \sim 2$ mm) and the time scale as the typical experimental time scale ($\tau_{ve} \approx 20$ ms), we get $Ec^* \approx 0.15$

$$\{\tfrac{1}{2}t\dot{r}^2 + \tfrac{1}{2}t^2\ddot{r} - r\dot{r}[F(\theta_0) + \cos(\theta_0)]\} = -\epsilon Ec^* r\dot{r}^2. \tag{5.4}$$

To address the viscoelastic case, we express the viscosity (in the high-shear-rate region) in (5.3) as $\eta(\dot{\gamma}) \approx \eta_0/(\tau_{ve}\dot{\gamma})^m = \epsilon\eta_0^*/\dot{\gamma}^m$. Note that we let η_0^* carry all the units and remaining numerical factors. Since mainly the high shear region close to the contact line contributes to the viscous dissipation (Huh & Scriven 1971; Li *et al.* 2023), only the high-shear-rate viscosity is considered here. By estimating the shear rate as a function of the contact line velocity as $\dot{\gamma} \simeq u_{cl}/d^*$ (d^* is the distance to the contact line), the viscous dissipation can be written as $j_e^D \simeq \eta^* r u^{2-m}$. With this assumption, the force balance equation (5.3) can be rewritten

$$\{\tfrac{1}{2}t\dot{r}^2 + \tfrac{1}{2}t^2\ddot{r} - r\dot{r}[F(\theta_0) + \cos(\theta_0)]\} = -\epsilon Ec_0^* r\dot{r}^{2-m}. \tag{5.5}$$

We use Mathematica (Wolfram Alpha Co. Version 10) to solve (5.4) and (5.5) numerically; see supplementary material for details. We start exploring the effect of the Newtonian and viscoelastic viscosity from the inviscid case discussed in Bird *et al.* (2008). For example, we consider the case in which the drop spreading follows $r(t) = 0.02t^{0.4}$ and $r(t) = 0.02t^{0.5}$, in our dimensionless units. The obtained solution is not exactly a power law, but close to it. We fitted the numerical results by a simple power law ($B't^{\alpha'}$), where B' and α' are the effective prefactor and exponent, respectively, for the case of $r(t) = 0.02t^{0.4}$ (figure 5*a*). These theoretical exponents are plotted in figure 5(*b*) as a function of the small parameter ϵ and the rheological exponent m. We consider that the elastocapillary numbers are equal in both cases, since in the experimental part we compare the drops with the same zero-shear viscosity. These results show that, in the viscoelastic case, the exponent decreases more strongly than in the Newtonian case, by increasing the m value (i.e. increasing the viscoelasticity of the samples). This agrees with the experimental observation (figure 3). For the second case ($r(t) = 0.02t^{0.5}$), the theoretical exponent is plotted vs the different values of m in (1.3), which is an indicator for the level of viscoelasticity (figure 6*a*). Also shown is the theoretical prefactor as a function of the effective viscosity ϵEc^*, which shows that, by increasing the zero-shear-rate viscosity, the prefactor decreases. This observation is also in line with our experimental observation.

It is worth mentioning that the first-order perturbation method is only valid for a small correction term. The prefactor of the perturbed term (ϵEc^*) is between zero and 0.01, which results in the zero-shear-rate viscosity being in the range of 0 to 7 mPa s. This means

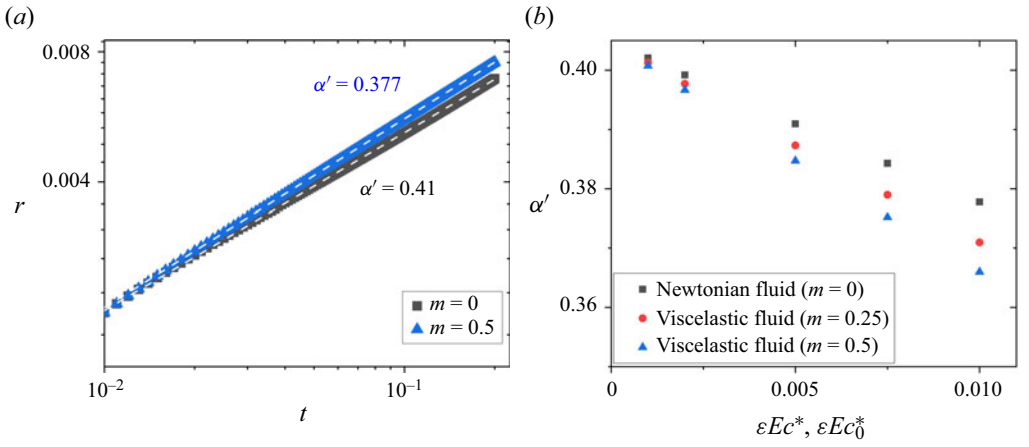

Figure 5. (*a*) Fitting of the numerical solution for different viscoelasticity levels ($m = 0$ and $m = 0.5$) for the case of $r(t) = 0.02t^{0.4}$. (*b*) The theoretical exponent (α') as a function of ϵEc^* values, for viscous Newtonian and viscoelastic fluids ($m = 0.25$ and $m = 0.5$), for the same case.

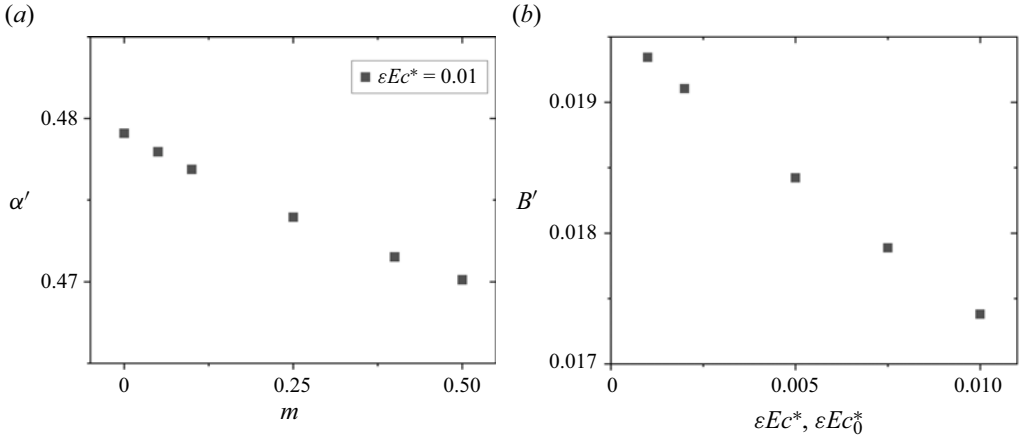

Figure 6. (*a*) The effect of viscoelasticity level (m) on the effective spreading exponent α' for a fixed value of $\epsilon Ec^* = 0.01$ for $r(t) = 0.02t^{0.5}$. (*b*) The theoretically predicted effective prefactor (B') vs the different effective viscosity ϵEc^* values.

that our model is only valid for very limited cases but represents the first steps toward the explanation of the experimental data. In summary, this simple perturbation analysis agrees with the main trends observed in the experiments (compare figure 4): (i) adding viscoelasticity to the system in terms of a shear-rate-dependent viscosity, the effective exponent (α') decreases; (ii) increasing the viscous dissipation (i.e. the perturbation term), the prefactor decreases. This simple proposed model shows the key features of the experimental tendencies.

6. Conclusion

The early stage spreading of Newtonian and viscoelastic fluids on hydrophilic and hydrophobic substrates has been studied. Generally speaking, viscoelastic drops spread faster compared with Newtonian drops with the same physical properties (zero-shear-rate

viscosity and surface tension). This difference can be justified by the fact that, near the contact line, the shear rate is extremely high. This leads to a decrease of the effective viscosity which is not the case for Newtonian liquids. To be able to observe the viscoelastic effect, the experimental time scale should be of the order of the internal relaxation time of the used polymer solution or longer. Therefore, for higher molar masses of the polymer, which corresponds to higher elastocapillary numbers, the time evolution of drop spreading in the experimental time scale ($\approx$20 ms) is independent of polymer concentration and molar mass and the spreading exponent is very close to the water case, i.e. the inviscid case. The influence of the viscoelasticity on drop spreading is especially pronounced when the polymer relaxation time (τ_{ve}) and the viscous–capillary time scale t_{vc} are similar, i.e. $Ec \approx 1$. These experimental observations can be supported by a simple first-order model for non-negligible but not too high viscosities. Future steps should include successively dropping the approximations made in our first-order model e.g. compare with a broader range of material parameters and experimental conditions. Since the presented first model is limited to the first few experimental data points, future steps should successively drop the approximations or include higher-order terms in the modelling. The results also confirm the dependency of the spreading exponent on the wettability of the substrate.

Supplementary material. Supplementary material are available at https://doi.org/10.1017/jfm.2024.450.

Funding. This study was funded by the Deutsche Forschungsgemeinschaft Project No. 265191195–SFB 1194, 'Interaction between Transport and Wetting Processes' and the Deutsche Forschungsgemeinschaft (DFG) Project No. 422852551, within the priority program SPP 2171.

Declaration of interest. The authors report no conflict of interest.

Author ORCIDs.
Peyman Rostami https://orcid.org/0000-0002-1066-966X;
Mathis Fricke https://orcid.org/0000-0002-6281-6617;
Simon Schubotz https://orcid.org/0000-0001-8659-7132;
Reza Azizmalayeri https://orcid.org/0000-0002-5113-8128;
Günter K. Auernhammer https://orcid.org/0000-0003-1515-0143.

References

Anna, S.L. & McKinley, G.H. 2001 Elasto-capillary thinning and breakup of model elastic liquids. *J. Rheol. (N.Y.)* **45** (1), 115–138.

Betelu, S.I. & Fontelos, M.A. 2003 Capillarity driven spreading of power-law fluids. *Appl. Maths Lett.* **16** (8), 1315–1320.

Biance, A.-L., Clanet, C. & Quéré, D. 2004 First steps in the spreading of a liquid droplet. *Phys. Rev.* E **69** (1), 016301.

Bird, J.C., Mandre, S. & Stone, H.A. 2008 Short-time dynamics of partial wetting. *Phys. Rev. Lett.* **100** (23), 234501.

Blake, T.D. & Haynes, J.M. 1969 Kinetics of liquid/ liquid displacement. *J. Colloid Interface Sci.* **30**, 421–423.

Bodziony, F., Wörner, M. & Marschall, H. 2023 The stressful way of droplets along single-fiber strands: a computational analysis. *Phys. Fluids* **35**, 012110.

Bonn, D., Eggers, J., Indekeu, J., Meunier, J. & Rolley, E. 2009 Wetting and spreading. *Rev. Mod. Phys.* **81** (2), 739.

Bouillant, A., Dekker, P.J., Hack, M.A. & Snoeijer, J.H. 2022 Rapid viscoelastic spreading. *Phys. Rev. Fluids* **7** (12), 123604.

Carlson, A., Bellani, G. & Amberg, G. 2011 Measuring contact line dissipation in dynamic wetting. Available at https://kth.diva-portal.org/smash/record.jsf?pid=diva2%3A422041&dswid=295.

Carlson, A., Bellani, G. & Amberg, G. 2012 Universality in dynamic wetting dominated by contact-line friction. *Phys. Rev.* E **85** (4), 045302.

CARRÉ, A. & EUSTACHE, F. 2000 Spreading kinetics of shear-thinning fluids in wetting and dewetting modes. *Langmuir* **16** (6), 2936–2941.
CARRÉ, A., GASTEL, J.-C. & SHANAHAN, M.E.R. 1996 Viscoelastic effects in the spreading of liquids. *Nature* **379** (6564), 432–434.
CARRÉ, A. & SHANAHAN, M.E.R. 2001 Viscoelastic braking of a running drop. *Langmuir* **17** (10), 2982–2985.
CHEN, L., AUERNHAMMER, G.K. & BONACCURSO, E. 2011 Short time wetting dynamics on soft surfaces. *Soft Matt.* **7** (19), 9084–9089.
CHEN, L., BONACCURSO, E. & SHANAHAN, M.E.R. 2013*a* Inertial to viscoelastic transition in early drop spreading on soft surfaces. *Langmuir* **29** (6), 1893–1898.
CHEN, L., LI, C., VAN DER VEGT, N.F.A., AUERNHAMMER, G.K. & BONACCURSO, E. 2013*b* Initial electrospreading of aqueous electrolyte drops. *Phys. Rev. Lett.* **110** (2), 026103.
CHERRY, B.W. & HOLMES, C.M. 1969 Kinetics of wetting of surfaces by polymers. *J. Colloid Interface Sci.* **29** (1), 174–176.
COSTANZO, S., HUANG, Q., IANNIRUBERTO, G., MARRUCCI, G., HASSAGER, O. & VLASSOPOULOS, D. 2016 Shear and extensional rheology of polystyrene melts and solutions with the same number of entanglements. *Macromolecules* **49** (10), 3925–3935.
COX, R.G. 1986 The dynamics of the spreading of liquids on a solid surface. Part 1. Viscous flow. *J. Fluid Mech.* **168**, 169–194.
CROSS, M.M. 1965 Rheology of non-Newtonian fluids: a new flow equation for pseudoplastic systems. *J. Colloid Sci.* **20** (5), 417–437.
DONTULA, P., MACOSKO, C.W. & SCRIVEN, L.E. 1999 Does the viscosity of glycerin fall at high shear rates? *Ind. Engng Chem. Res.* **38** (4), 1729–1735.
DU, J., CHAMAKOS, N.T., PAPATHANASIOU, A.G. & MIN, Q. 2021 Initial spreading dynamics of a liquid droplet: the effects of wettability, liquid properties, and substrate topography. *Phys. Fluids* **33** (4), 042118.
EDDI, A., WINKELS, K.G. & SNOEIJER, J.H. 2013 Short time dynamics of viscous drop spreading. *Phys. Fluids* **25** (1), 013102.
EGGERS, J., LISTER, J.R. & STONE, H.A. 1999 Coalescence of liquid drops. *J. Fluid Mech.* **401**, 293–310.
FERMIGIER, M. & JENFFER, P. 1991 An experimental investigation of the dynamic contact angle in liquid-liquid systems. *J. Colloid Interface Sci.* **146** (1), 226–241.
FOX, H.W. & ZISMAN, W.A. 1950 The spreading of liquids on low energy surfaces. I. Polytetrafluoroethylene. *J. Colloid Sci.* **5** (6), 514–531.
FRICKE, M. & BOTHE, D. 2020 Boundary conditions for dynamic wetting-a mathematical analysis. *Eur. Phys. J. Spec. Topics* **229** (10), 1849–1865.
FRICKE, M., KÖHNE, M. & BOTHE, D. 2019 A kinematic evolution equation for the dynamic contact angle and some consequences. *Phys. D: Nonlinear Phenom.* **394**, 26–43.
GASTONE, F., TOSCO, T. & SETHI, R. 2014 Green stabilization of microscale iron particles using guar gum: bulk rheology, sedimentation rate and enzymatic degradation. *J. Colloid Interface Sci.* **421**, 33–43.
DE GENNES, P.G. 1985 Wetting: statics and dynamics. *Rev. Mod. Phys.* **57** (3), 827.
GLASSER, A., CLOUTET, E., HADZIIOANNOU, G. & KELLAY, H. 2019 Tuning the rheology of conducting polymer inks for various deposition processes. *Chem. Mater.* **31** (17), 6936–6944.
HARDY, W.B. 1919 III. The spreading of fluids on glass. *Lond. Edinb. Dublin Phil. Mag. J. Sci.* **38** (223), 49–55.
HARTMANN, M., FRICKE, M., WEIMAR, L., GRÜNDING, D., MARIĆ, T., BOTHE, D. & HARDT, S. 2021 Breakup dynamics of capillary bridges on hydrophobic stripes. *Intl J. Multiphase Flow* **140**, 103582.
HOATH, S.D. 2016 *Fundamentals of Inkjet Printing: The Science of Inkjet and Droplets*. John Wiley & Sons.
HUH, C. & MASON, S.G. 1977 The steady movement of a liquid meniscus in a capillary tube. *J. Fluid Mech.* **81** (3), 401–419.
HUH, C. & SCRIVEN, L.E. 1971 Hydrodynamic model of steady movement of a solid/liquid/fluid contact line. *J. Colloid Interface Sci.* **35** (1), 85–101.
IWAMATSU, M. 2017 Spreading law of non-Newtonian power-law liquids on a spherical substrate by an energy-balance approach. *Phys. Rev.* E **96** (1), 012803.
JALAAL, M., STOEBER, B. & BALMFORTH, N.J. 2021 Spreading of viscoplastic droplets. *J. Fluid Mech.* **914**, A21.
LI, X., BODZIONY, F., YIN, M., MARSCHALL, H., BERGER, R. & BUTT, H.-J. 2023 Kinetic drop friction. *Nat. Commun.* **14**, 4571.
LIANG, Z.-P., WANG, X.-D., LEE, D.-J., PENG, X.-F. & SU, A. 2009 Spreading dynamics of power-law fluid droplets. *J. Phys.: Condens. Matter* **21** (46), 464117.

McKinley, G.H. 2005 Dimensionless groups for understanding free surface flows of complex fluids. Available at https://web.mit.edu/nnf/publications/GHM78.pdf.

Moffatt, H.K. 1964 Viscous and resistive eddies near a sharp corner. *J. Fluid Mech.* **18** (01), 1–18.

Muralidhar, P., Bonaccurso, E., Auernhammer, G.K. & Butt, H.-J. 2011 Fast dynamic wetting of polymer surfaces by miscible and immiscible liquids. *Colloid Polym. Sci.* **289** (14), 1609–1615.

Pelosse, A., Guazzelli, É. & Roché, M. 2023 Probing dissipation in spreading drops with granular suspensions. *J. Fluid Mech.* **955**, A7.

Petrov, J.G., Ralston, J., Schneemilch, M. & Hayes, R.A. 2003 Dynamics of partial wetting and dewetting in well-defined systems. *J. Phys. Chem.* B **107** (7), 1634–1645.

Rednikov, A.Y. & Colinet, P. 2012 Evaporation-driven contact angles in a pure-vapor atmosphere: the effect of vapor pressure non-uniformity. *Math. Model. Nat. Phenom.* **7** (4), 53–63.

Rostami, P., Hormozi, M.A., Soltwedel, O., Azizmalayeri, R., von Klitzing, R. & Auernhammer, G.K. 2023 Dynamic wetting properties of pdms pseudo-brushes: four-phase contact point dynamics case. *J. Chem. Phys.* **158**, 194703.

Ruckenstein, E. & Dunn, C.S. 1977 Slip velocity during wetting of solids. *J. Colloid Interface Sci.* **59** (1), 135–138.

Sankaran, A.K. & Rothstein, J.P. 2012 Effect of viscoelasticity on liquid transfer during gravure printing. *J. Non-Newtonian Fluid Mech.* **175–176**, 64–75.

Shanahan, M.E.R. 2001 Condensation transport in dynamic wetting. *Langmuir* **17** (13), 3997–4002.

Shikhmurzaev, Y.D. 1997 Moving contact lines in liquid/liquid/solid systems. *J. Fluid Mech.* **334**, 211–249.

Shikhmurzaev, Y.D. 2020 Moving contact lines and dynamic contact angles: a 'litmus test' for mathematical models, accomplishments and new challenges. *Eur. Phys. J. Spec. Topics* **229** (10), 1945–1977.

Shuttleworth, R. & Bailey, G.L.J. 1948 The spreading of a liquid over a rough solid. *Discuss. Faraday Soc.* **3**, 16–22.

Snoeijer, J.H. & Andreotti, B. 2013 Moving contact lines: scales, regimes, and dynamical transitions. *Annu. Rev. Fluid Mech.* **45** (1), 269–292.

Snoeijer, J.H., Rio, E., Le Grand, N. & Limat, L. 2005 Self-similar flow and contact line geometry at the rear of cornered drops. *Phys. Fluids* **17**, 072101.

Subbaraman, V., Mashelkar, R.A. & Ulbrecht, J. 1971 Extrapolation procedures for zero shear viscosity with a falling sphere viscometer. *Rheol. Acta* **10**, 429–433.

Tanner, L.H. 1979 The spreading of silicone oil drops on horizontal surfaces. *J. Phys.* D*: Appl. Phys.* **12** (9), 1473.

Vereroudakis, E., Van Zee, N., Meijer, E.W. & Vlassopoulos, D. 2023 Repeated shear startup response of a supramolecular polymer. *J. Non-Newtonian Fluid Mech.* **315**, 105021.

Voinov, O.V. 1976 Hydrodynamics of wetting. *Fluid Dyn.* **11** (5), 714–721.

Wayner, P.C. 1994 Mechanical and thermal effects in the forced spreading of a liquid film with a finite contact angle. *Colloids Surf.* A*: Physicochem. Engng Aspects* **89** (2), 89–95.

Worthington Arthur, M. & Reynolds, O. 1883 On impact with a liquid surface. *Proc. R. Soc. Lond.* **34** (220-223), 217–230.

Yada, S., Bazesefidpar, K., Tammisola, O., Amberg, G. & Bagheri, S. 2023 Rapid wetting of shear-thinning fluids. *Phys. Rev. Fluids* **8** (4), 043302.

Young, T. 1805 III. An essay on the cohesion of fluids. *Phil. Trans. R. Soc. Lond.* **1**, 171–172.

Zhao, B., Bonaccurso, E., Auernhammer, G.K. & Chen, L. 2021 Elasticity-to-capillarity transition in soft substrate deformation. *Nano Lett.* **21** (24), 10361–10367.